Arabian Journal of Chemistry (2017) **10**, 1147–1152

King Saud University

Arabian Journal of Chemistry

www.ksu.edu.sa
www.sciencedirect.com

ORIGINAL ARTICLE

Effect of water-based sol gel method on structural, thermal and conductivity properties of $LiNO_3$–Al_2O_3 composite solid electrolytes

M. Sulaiman *, **A.A. Rahman, N.S. Mohamed**

Centre for Foundation Studies in Science, University of Malaya, 50603 Kuala Lumpur, Malaysia

Received 19 July 2013; accepted 23 April 2015
Available online 4 May 2015

KEYWORDS

Composite material;
Conductivity;
Lithium nitrate;
Alumina composite

Abstract Composite solid electrolytes in the system $(1-x)LiNO_3$–xAl_2O_3, with x = 0.0–0.5 were prepared by sol gel method. No organic solvents but water was used as medium for the sol preparation. The obtained materials were characterized by X-ray diffraction, differential scanning calorimetry, scanning electron microscopy, Fourier transform infrared spectroscopy and impedance spectroscopy. Structural analysis evidenced amorphous phase of $LiNO_3$ in all composite samples. Traces of crystalline $LiAl_5O_8$ and $LiAlO_2$ were also present in the composite samples with x = 0.3–0.5, as indicated by the X-ray diffractograms. The thermal analysis showed that the samples were in a stable phase between ~48 °C – ~100 °C and ~120 °C – ~220 °C. The conductivity values of the composites were in the range of 10^{-3} S cm^{-1} at room temperature to 180 °C. Our study demonstrates that water is suitable for the preparation of the composite solid electrolytes.

1. Introduction

The fast development and extensive application of electronic products, especially in automotive use and portable electronics require safe solid-state secondary batteries with high energy (Tarascon and Armand, 2001; Minami et al., 2005). For instance, lithium ion solid-state batteries are current power sources of choice due to their light weight, high voltage and high value of energy content and have contributed to the manufacture of countless electronic products (Scrosati and Garche, 2010). Solid-state batteries have both solid electrodes and electrolytes with good ion conductors for high power density. Solid electrolytes can be crystalline–polycrystalline, glassy-amorphous, composite and polymeric (Agrawal and Gupta, 1999). Composite solid electrolytes started to draw interest since the observation of enhanced ionic conductivity by Liang, 1973. Since then, both physical and chemical properties of composite solid electrolytes have been studied and the presence of number of surfaces and defect formation at free surfaces and interfaces in composites are main factor of conductivity enhancement (Uvarov and Vanek, 2000; Yaroslavtsev, 2009; Sulaiman et al., 2011, 2012). Uvarov observed that their structure could be either epitaxial crystalline or amorphous (Uvarov and Vanek,

* Corresponding author. Tel.: +603 79675918.
E-mail address: mazdidas@um.edu.my (M. Sulaiman).
Peer review under responsibility of King Saud University.

Production and hosting by Elsevier

http://dx.doi.org/10.1016/j.arabjc.2015.04.031
1878-5352

2000). In 1979, Wagner et al. (Jow and Wagner, 1979) reported that conductivity enhancement in a binary system MX-Al_2O_3 was associated with high concentration of defects in the ionic salts, MX containing mobile ions, M^+. Strong surface interaction of ionic salts with oxide leads to the spreading of MX over the surface of oxide and at adequately high oxide dispersity and concentration, the whole volume of the ionic salt turns into either a surface disordered state or an amorphous phase (Uvarov, 2000, 2011). These phenomena have been ascertained in our previous work on composite solid electrolytes in the system $(1-x)LiNO_3$–xAl_2O_3 with x = 0.0–0.5 based on ethanol sol gel method (Sulaiman et al., 2012). In this method, higher ionic conductivity values in the order of 10^{-3} S cm^{-1} at room temperature were obtained compared to the conductivity values around 10^{-5} S cm^{-1} (at 70 °C) for the same composite system prepared using mechanical milling (Uvarov et al., 1996a; Sulaiman et al., 2012). Here, we report the preparation of composite solid electrolytes in the system $(1-x)LiNO_3$–xAl_2O_3 using water-based sol gel technique instead of ethanol based sol–gel and investigate their structural, thermal and conductivity properties. Structural characterizations were carried out by X-ray diffraction (XRD), differential scanning calorimetry (DSC), scanning electron microscopy (SEM) and Fourier transform infrared spectroscopy (FTIR). The conductivity study was determined by alternating current (AC) impedance measurements. Our study demonstrates for the first time that deionized water which is both environmental friendly and economical, is suitable for the preparation of $(1-x)LiNO_3$–xAl_2O_3 with x = 0.0–0.5 composite solid electrolytes with high conductivity at room temperature.

2. Experimental

Composite solid electrolytes in the system $(1-x)LiNO_3$–xAl_2O_3 with x = 0.1–0.5 mol were synthesized by sol gel method. $LiNO_3$ (purity >99.0%, Fluka) and Al_2O_3 (purity >99.7%, Sigma Aldrich) were used as purchased without further purification. First, $LiNO_3$ was dissolved in deionized water and Al_2O_3 was then added to the solution. The solution was continuously stirred at 40 °C for 20 min. Consequently, to the solution was added citric acid and the mixture was heated at 80 °C on a hot plate with continuous stirring until the formation of a wet gel. The wet gel was then fully dried in oven at 220 °C. The final product obtained was fluffy and brown. Structural characterizations for XRD, FTIR and SEM were performed on a D8 Advanced-Bruker X-ray Diffractometer with Cu Kα radiation, a Perkin Elmer RX1 spectrometer and INCA Energy 200 (Oxford Ins.), respectively. The thermal properties of the samples were measured on a Mettler Toledo DSC 822 with continuous heating at a rate of 10 °C min^{-1}. For conductivity studies, pellets were made by pressing the composite powders at a pressure of 6–8 tones cm^{-2}. The diameters of the pellets were 13 mm and their thicknesses were about 1.1 mm. The pellets were then sandwiched between two electrodes of a sample holder. Conductivities were measured by impedance spectroscopy on Solatron 1260 impedance analyzer at room temperature to 200 °C. An ac amplitude of 100 mV in the frequency range of 10^{-1}–10^7 Hz was used.

3. Results and discussion

3.1. XRD analysis

Fig. 1 shows XRD spectra for the pure $LiNO_3$ and composite samples of $(1-x)LiNO_3$–xAl_2O_3. The diffraction peaks at 2θ of 25.7°, 35.3°, 37.8°, 43.5°, 52.6°, 59.4°, 61.4°, 66.5°, 68.6° and 76.9° observed in the spectra of composite samples with x = 0.1–0.5 were attributed to Al_2O_3. Only one peak of very low intensity of $LiNO_3$ appeared at $2\theta \approx 25°$ for all composite samples, except in sample with x = 0.4. The absence of some $LiNO_3$ peaks in the XRD spectra corresponds to the existence of either crystalline and amorphous phases of $LiNO_3$ or a mesophase phase (Uvarov, 2011). At x = 0.4, the crystalline $LiNO_3$ was fully transformed into amorphous state. At the same time, weak reflection appeared at $2\theta \approx 22°$ in the spectra of the samples with x = 0.3–0.4 and was assigned to crystalline $LiAl_5O_8$. At x = 0.3–0.5, the diffraction peaks appeared at $2\theta \approx 29°$, $\approx 32°$ and $\approx 34°$ and were ascribed to $LiAlO_2$. The XRD spectra for composite samples with x = 0.3–0.5 showed that chemical reactions took place between $LiNO_3$ and Al_2O_3 during the sol gel preparation to produce traces of crystalline $LiAl_5O_8$ and $LiAlO_2$ (lithium aluminates). The transformation of the interaction in the composite samples can be represented by the following route (Sulaiman et al., 2012; Oksuzomer et al., 2004; Valenzuela et al., 2001):

$$\text{Lithium nitrate} + \text{alumina} \rightarrow \text{amorphous} + LiAl_5O_8 + LiAlO_2$$

In earlier work, the $LiAl_5O_8$ phase was not detected (Sulaiman et al., 2012). This can be explained by the high degree of solubility of $LiNO_3$ in water than that in ethanol.

3.2. DSC analysis

DSC curves of the composite $(1-x)$ $LiNO_3$–xAl_2O_3 samples are shown Fig. 2. An endothermic peak was observed at 100 °C and was attributed to dehydration. A stable phase for the composite system (x = 0.1–0.5) appeared between ~120 °C and ~200 °C. An endothermic peak around 220 °C

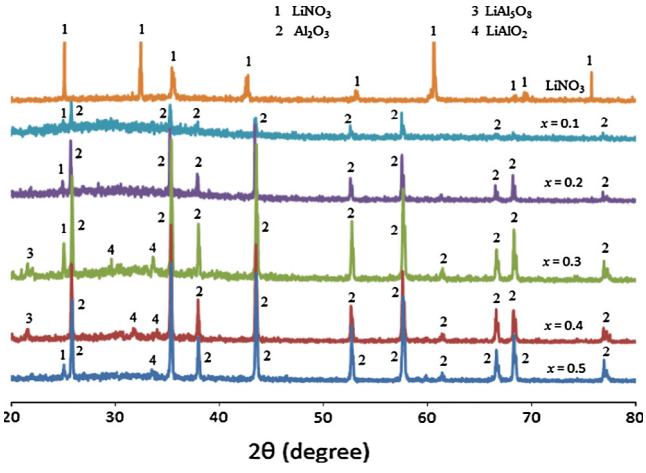

Figure 1 XRD patterns of $(1-x)$ $LiNO_3$–xAl_2O_3 composites.

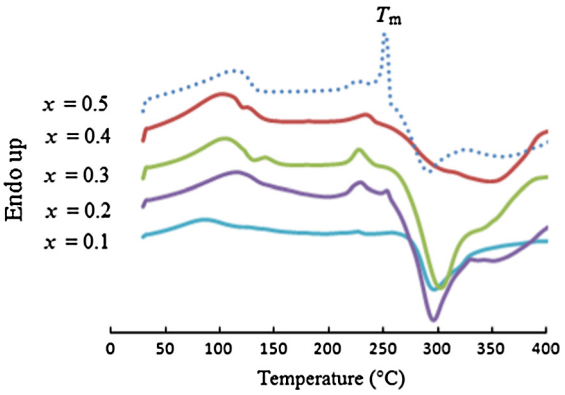

Figure 2 DSC scanning of $(1-x)LiNO_3$–xAl_2O_3 composites.

was attributed to the decomposition of citric acid. Another endothermic peak at 252 °C was attributed to the melting of $LiNO_3$ (T_m) (Ribeiro et al., 2001). There was no melting point of crystalline $LiNO_3$ found in the composite sample with $x < 0.5$. This phenomenon could be attributed to the phase change of crystalline $LiNO_3$ to amorphous and mesophase phases that occurred due to the application of heat closed to the melting point of pure $LiNO_3$ during the preparation of the samples (Uvarov, 2011). At this state, the long-range and rigid ordering of crystalline $LiNO_3$ breaks down to a less ordered state, thereby promoting the Li^+ ion mobility in the composites. The exothermic peaks at ~290 °C – ~350 °C in all composite samples were related to the thermal decomposition of $LiNO_3$ and the formation of lithium aluminates (Chatterjee and Naskar, 2003; Oksuzomer et al., 2004). There was no exothermic curve of the formation of lithium aluminates found for composite sample with $x = 0.1$.

3.3. FTIR analysis

FTIR spectra of $LiNO_3$ ($x = 0.0$) and composite samples with $x = 0.1$–0.5 in the wavenumber range 1500–500 cm^{-1} are presented Fig. 3(a). The very strong absorption band in the spectra of pure $LiNO_3$ at 1384 cm^{-1} and the medium bands at 1051 cm^{-1} and 827 cm^{-1} were ascribed to the asymmetric stretching mode, symmetric stretching mode and out of plane deformation mode of NO_3^- ions, respectively (Chatterjee et al., 1998, 2002; Kamiya et al., 1991; Nakamoto, 1978; Tamura et al., 2004; Gaphurov and Aliev, 1999). These characteristic bands of nitrate groups appeared at 1389–1402 and 825–827 cm^{-1} in all spectra of the composite samples demonstrating that $LiNO_3$ phase was present in all of the composite samples ($x = 0.1$–0.5).

As can be seen in Fig. 3(b), there was a small asymmetric distortion in the contour of symmetric stretching mode band of NO_3^- for the composite sample with $x = 0.4$. The bandwidth of the vibration band became broader and the position was slightly shifted to 1050 cm^{-1}. The contour band of the symmetric stretching mode was inconspicuous for composite samples with $x = 0.1$, 0.2, 0.3 and 0.5. This effect was due to the heating of the sample up to a temperature ~30 °C below the melting point of pure $LiNO_3$ allowing the formation of fully amorphous phase of $LiNO_3$ (Uvarov, 2011). Gaphurov et al. (2002) reported that the distortion was related to the orientation disordered anions of NO_3^- anions in the $LiNO_3$ crystal lattice. A similar observation was reported in $RbNO_3$–Al_2O_3 nanocomposite, where the position of absorption peaks in a disordered state was observed at lower wavenumber and broadened (Uvarov et al., 1996b).

The complex structure of asymmetric stretching mode band at 1389 cm^{-1} of the spectra of composite samples with $x = 0.3$–0.5 was attributed to interaction between nitrates and alumina particles. As discussed in Section 3.1, traces of crystalline $LiAl_5O_8$ and $LiAlO_2$ were formed in these composite samples. The vibration bands of Al–O bonds could be observed in the infrared region between 900 and 500 cm^{-1} (Chatterjee and Naskar, 2003; Boumaza et al., 2009). The bands at 550 and 636 cm^{-1} observed in Fig. 3(a) corresponded from AlO_6 stretching modes and were linked to α-Al_2O_3 (Boumaza et al., 2009). Bands at 642, 544 and 520 cm^{-1} in composite samples with $x = 0.3$–0.5 referred to AlO_4–LiO_4 lattice of the $LiAlO_2$ and $LiAl_5O_8$ phases (Oksuzomer et al., 2004; Li et al., 2002). The bands appeared at 610 and 680 cm^{-1} corresponding to $LiAl_5O_8$ phase could be clearly be seen in composite sample with $x = 0.3$ (Oksuzomer et al., 2004; Ribeiro et al., 2001). The changes in the spectral properties in the nitrates could be attributed to the rotary mobility of molecular ion due to substantial thermal activation and the increase in dynamic interaction between the ions that occurred during the sample preparation (Gaphurov et al., 2002).

3.4. SEM analysis

Fig. 4 shows SEM micrographs of composite sample with $x = 0.4$. As observed from Fig. 4(a), only alumina particles dominantly appeared in the composite sample. On the contrary, the $LiNO_3$ (dark region) was observed to be in the amorphous form and apparently spreading over the alumina particle surface. The spreading of lithium nitrate over the surface of the oxide was the main factor to the formation of the amorphous phase of lithium nitrate. The ionic salt was expected to spread only in a molten state which occurred at temperatures closed to T_m. The amorphous phase was formed as the result of the ionic melt and physical interaction of both Al_2O_3 and $LiNO_3$ crystalline phases (Uvarov et al., 1996b; Neiman et al., 2007). According to Uvarov and Vanek (2000), amorphous phase may be formed at the interface phase when composites obtained are in strong nonequilibrium conditions or if the surface structures of ionic salts and oxide are very different. Fig. 4(b) shows that alumina particles (white region) were uniformly dispersed in the composite mixture confirming thus interfacial interaction between both Al_2O_3 and $LiNO_3$ crystalline phases.

3.5. Electrical conductivity

Complex impedance plots of composite samples with $x = 0.1$–0.3 and $x = 0.4$–0.5 are shown in Figs. 5 and 6, respectively. For composite samples with x–0.1–0.3, the plots show a slanted spike at low frequency and distorted semicircles at higher frequencies. The formation of spike represented interfacial effects between electrode and electrolyte (Dygas et al., 2005; Godinho et al., 2003). The high and low frequency semicircles with the interception at the Z'-axis were assigned to bulk resistance (R_b) and grain boundary resistance (R_{gb}),

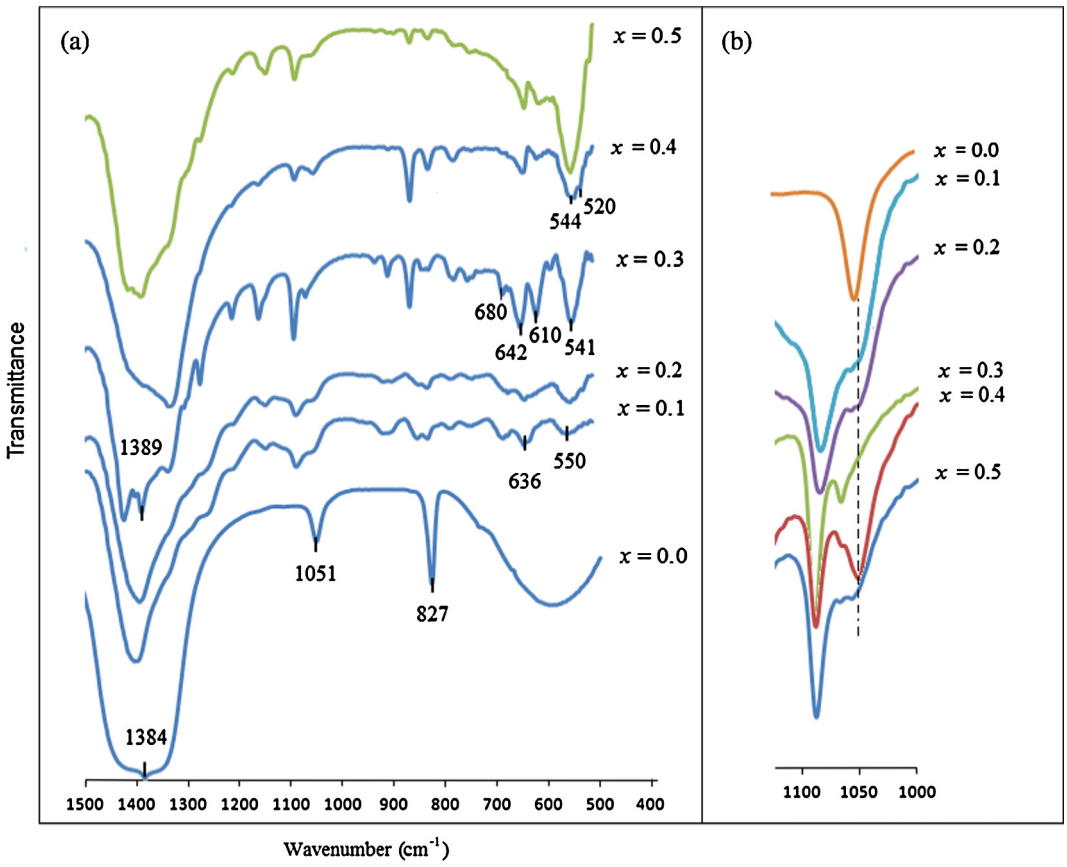

Figure 3 FTIR spectra of $(1-x)LiNO_3$–xAl_2O_3 composites in (a) 500–1500 cm^{-1} and (b) 1100–1000 cm^{-1} regions.

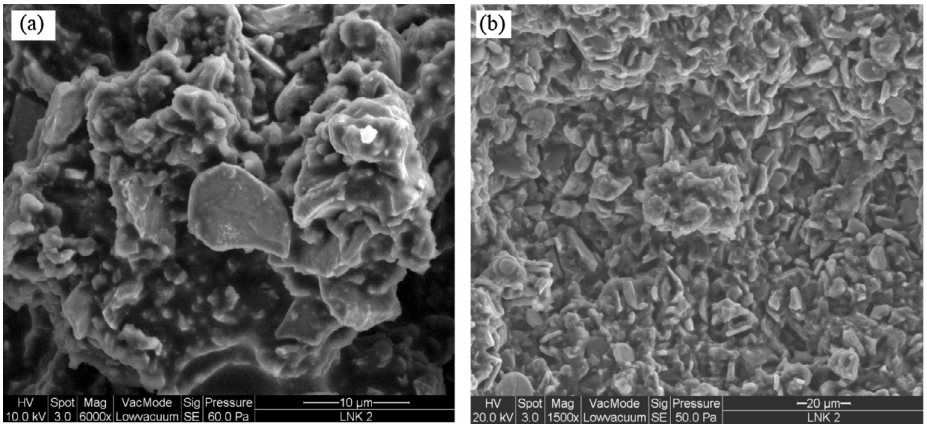

Figure 4 Morphologies of composite sample with $x = 0.4$ magnified at (a) 6000× and (b) 1500×.

respectively. The appearance of these two semicircles could be associated with different conduction process in the composite samples. The ionic conduction could be occurring through the grain and along the grain boundaries of $LiNO_3$. However, the semicircle portion at higher frequency disappeared with increase in alumina composition, as shown in impedance plot for composite samples with $x = 0.4$–0.5 (Fig. 6). The disappearance of semicircle portion implied that only resistive components prevailed in the composite samples. In this case, alumina particles were the only resistive component, as clearly shown in the SEM micrographs in Fig. 4. In the present work, by knowing the value of bulk resistance (R_b), the conductivity has been calculated using the relationship as shown below:

$$\sigma = \frac{d}{R_b A} \tag{1}$$

where d is the sample thickness (cm), R_b is bulk resistance (Ω), and A is the area (cm^2) of the sample.

Fig. 7 shows the compositional dependence of conductivity at room temperature (25 °C) for pure $LiNO_3$ and $(1-x)LiNO_3$–xAl_2O_3 composite samples. The conductivity

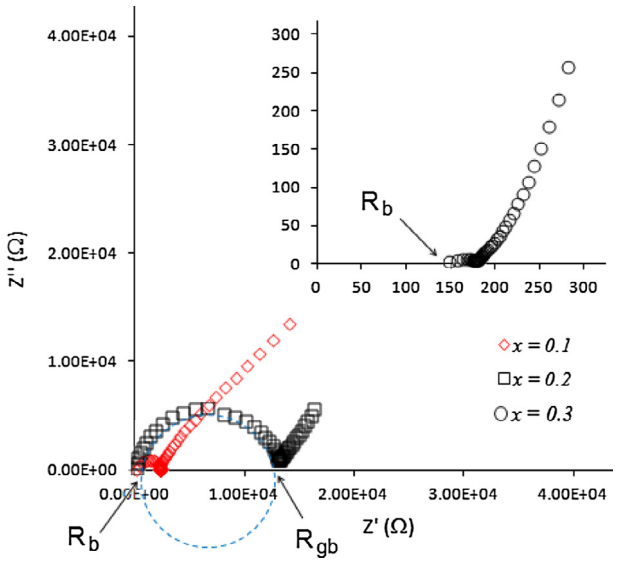

Figure 5 Complex impedance plot of composite samples with $x = 0.1$, 0.2 and 0.3 at room temperature.

dependence plot had two maxima at $x = 0.1$ and $x = 0.4$. The conductivities were found to increase from $x = 0.0$ to 0.1 but decreased steadily with further increase in x. However, beyond the composite samples with $x = 0.2$, the conductivity slowly increased up to $x = 0.4$. From Fig. 7, it was observed that the conductivity decreased again after the maximum point of $x = 0.4$. The enhancement in ionic conductivity in the composite sample with $x = 0.1$ was due to the formation of the amorphous phase of $LiNO_3$, as indicated by the XRD and DSC results, in Figs. 1 and 2, respectively. The collapse of $LiNO_3$ crystal lattice initiated the orientational disordered anions of NO_3^- and consequently increased the number of Li^+ ions. It suggests that the ionic conductivity proceeded via amorphous interface phase (Gaphurov et al., 2002; Uvarov et al., 1996a; Rao et al., 2005). Decrease in conductivity for composite samples with $x > 0.1$ could be explained by the increasing amount of alumina (dispersoid) grains in the composites which reduced the surface area of contact between the host matrix of $LiNO_3$ and the dispersoid grains. This led to the blocking effect by the alumina grains that hinder the migration of the Li^+ ions. Beyond $x = 0.2$, however, the conductivity continued to increase due to the presence of new phases of $LiAlO_2$ and $LiAl_5O_8$ in the composite samples with $x = 0.3$–0.5. The highest conductivity value of 1.97×10^{-3} S cm^{-1} occurred in the composite sample with $x = 0.4$. The high ionic conductivity in this composite sample was related to the presence of the fully amorphous phase of $LiNO_3$ as revealed by the XRD spectra and the spreading of the $LiNO_3$ over the alumina as shown in the SEM micrograph in Fig. 4. The high ionic conductivity around 10^{-3} S cm^{-1} at room temperature has also been observed for the same composite solid electrolyte system prepared using ethanol (Sulaiman et al., 2012). It means that the water-based system of the prepared composite samples is able to produce materials with high ionic conductivity.

Temperature dependencies of conductivity for $(1-x)LiNO_3$–xAl_2O_3 composites prepared are shown in Fig. 8. Conductivities values of the composite samples increased with temperature. Interestingly, the composite samples exhibited conductivities in the same range of 10^{-3} S cm^{-1} at room temperature to 180 °C (except $x = 0.2$). As discussed earlier, the amorphous phase of the $LiNO_3$ played a major role in conductivity enhancement in composite samples. Beginning at a temperature of 110 °C, conductivities continued to be constant (except $x = 0.2$). This was due to stable state between 110 °C and 200 °C as shown in the DSC curves. The low ionic conductivity in composite sample with $x = 0.2$ could be related to the absence of crystalline $LiAlO_2$ and $LiAl_5O_8$, which on the other hand, enhanced the conductivity of the composite samples with $x = 0.3$–0.5. The activation energy was obtained by fitting the ionic conductivity data with Arrhenius equation:

$$\sigma = A \exp\left(\frac{-E_a}{kT}\right) \tag{2}$$

where A is the pre-exponential factor, E_a is the activation energy for conduction and k is the Boltzmann's constant which is 8.52×10^{-5} eV/kelvin, T is the temperature in Kelvin. The activation energy for all samples is shown in Fig. 8. The low value of activation energy indicates high mobility of ions in the sample.

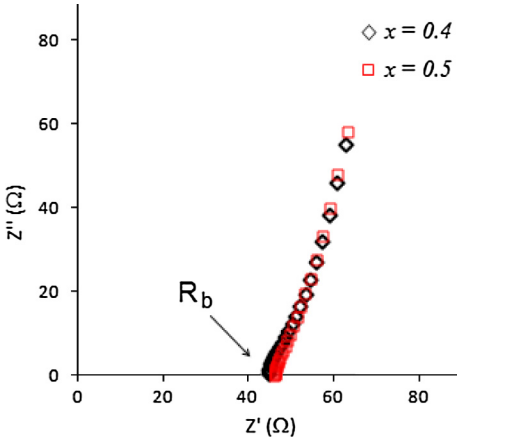

Figure 6 Complex impedance plot of composite samples with $x = 0.4$ and 0.5 at room temperature.

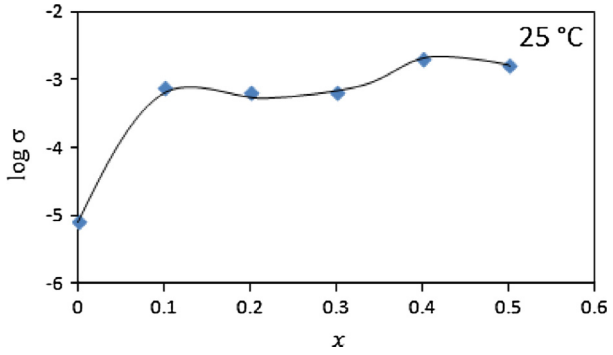

Figure 7 The ionic conductivity as a function of composition (x) for composites $(1-x)$ $LiNO_3$–xAl_2O_3 at room temperature.

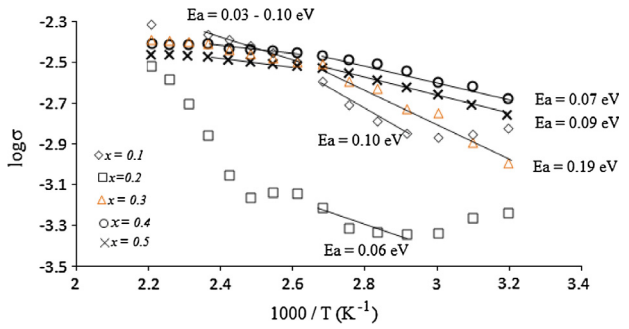

Figure 8 Temperature dependence of the conductivity of $(1-x)LiNO_3$–xAl_2O_3 composites.

4. Conclusions

Our study demonstrate for the first time that composite solid electrolytes in the system $(1-x)LiNO_3$–xAl_2O_3 with $x = 0.0$–0.5 prepared by sol–gel method using solely deionized water as medium for sol preparation exhibited high ionic conductivity at room temperature and especially at $x = 0.4$.

Acknowledgment

The authors would like to thank the University of Malaya for granting the Research Grant (RG021/09AFR) to support this work.

References

Agrawal, R.C., Gupta, R.K., 1999. Review superionic solids: composite electrolyte phase-an overview. J. Mater. Sci. 34, 1131–1162.

Boumaza, A., Favaro, L., Ledion, J., Sattonnay, G., Brubach, J.B., Berthet, P., Huntz, A.M., Roy, P., Tetot, R., 2009. Transition alumina phases induced by heat treatment of boehmite: an X-ray diffraction and infrared spectroscopy study. J. Solid State Chem. 182, 1171–1178.

Chatterjee, M., Naskar, M.K., 2003. Novel technique for the synthesis of lithium aluminate ($LiAlO_2$) powders from water-based sols. J. Mater. Sci. Lett. 22, 1747–1749.

Chatterjee, M., Enkhtuvshin, D., Siladitya, B., Ganguli, D., 1998. Hollow alumina microspheres from boehmite Sols. J. Mater. Sci. 33, 4937–4942.

Chatterjee, M., Naskar, M.K., Lakshmi, N.S., 2002. Sol-emulsion-gel synthesis of hollow mullite microspheres. J. Mater. Sci. 37, 343–348.

Dygas, J.R., Malys, M., Krok, F., Wrobel, W., Kozanecka, A., Abrahams, I., 2005. Polycrystalline BIMGVOX.13 studied by impedance spectroscopy. Solid State Ionics 176, 2085–2093.

Gaphurov, M.M., Aliev, A.R., 1999. Raman and infrared spectroscopic studies of the platinum electrode/molten nitrate interface. Spectrochim. Acta Part A 55, 1237–1241.

Gaphurov, M.M., Aliev, A.R., Akhmedov, I.R., 2002. Raman and infrared study of the crystals with molecular anions in the region of a solid–liquid phase transition. Spectrochim. Acta Part A 58, 2683–2692.

Godinho, M.J., Bueno, P.R., Orlandi, M.O., Leite, E.R., Long, E., 2003. Ionic conductivity of $Bi_4Ti_{0.2}V_{1.8}O_{10.7}$ polycrystalline ceramics obtained by the polymeric precursor route. Mater. Lett. 57, 2540–2544.

Jow, T., Wagner, J.B., 1979. The effect of dispersed alumina particles on the electrical conductivity of cuprous chloride. J. Electrochem. Soc. 126, 1963–1972.

Kamiya, K., Takahashi, K., Maeda, T., Nasu, H., Yoko, T., 1991. Sol–gel derived CaO- and CeO_2- stabilized ZrO_2 fibres conversion process of gel to oxide and tensile strength. J. Eur. Ceram. Soc. 7, 295–305.

Li, F., Hu, K., Li, J., Zhang, D., Chen, G., 2002. Combustion synthesis of γ-lithium aluminate by using various fuels. J. Nucl. Mater. 300, 82–88.

Liang, C.C., 1973. Conduction characteristics of the lithium iodide – aluminium oxide solid electrolytes. J. Electrochem. Soc. 120, 1289–1292.

Minami, T., Tatsumisago, M., Wakihara, M., Iwakura, C., Kohjiya, S., Tanaka, I., 2005. Solid State Ionics for Batteries. Springer.

Nakamoto, K., 1978. Infrared and Raman spectra of inorganic and coordination compounds. Wiley, New York.

Neiman, A.Y., Uvarov, N.F., Pestereva, N.N., 2007. Solid state surface and interface spreading: an experimental study. Solid State Ionics 177, 3361–3369.

Oksuzomer, F., Koc, S.N., Boz, I., Gurkaynak, M.A., 2004. Effect of solvents on the preparation of lithium aluminate by sol–gel method. Mater. Res. Bull. 39, 715–724.

Rao, M.V.M., Reddy, S.N., Chary, A.S., 2005. DC ionic conductivity of $NaNO_3$:γ- Al_2O_3 composite solid electrolyte system. Physica B 362, 193–198.

Ribeiro, R.A., Silva, G.G., Mohallem, N.D.S., 2001. The influences of heat treatment on the structural properties of lithium aluminates. J. Phys. Chem. Solids 62, 857–864.

Scrosati, B., Garche, J., 2010. Review lithium batteries: status, prospects and future. J. Power Sources 195, 2419–2430.

Sulaiman, M., Rahman, A.A., Mohamed, N.S., 2011. Li_2CO_3–Al_2O_3 composite solid electrolytes prepared by sol gel method. Key Eng. Mater. 471–472, 379–384.

Sulaiman, M., Rahman, A.A., Mohamed, N.S., 2012. Sol–gel synthesis and characterization of $LiNO_3$–Al_2O_3 composite solid electrolyte. Solid State Sci. 14, 127–132.

Tamura, S., Mori, A., Imanaka, N., 2004. Li^+ ion conduction in (Gd, $La)_2O_3$–$LiNO_3$ system. Solid State Ionics 175, 467–470.

Tarascon, J.M., Armand, M., 2001. Issues and challenges facing rechargeable lithium batteries. Nature 414, 359–367.

Uvarov, N.F., 2000. Stabilization of amorphous phases in ion-conducting composites. Russ. J. Appl. Chem. 73, 1030–1035.

Uvarov, N.F., 2011. Composite solid electrolytes: recent advances and design strategies. J. Solid State Electrochem. 15, 367–389.

Uvarov, N.F., Vanek, P., 2000. Stabilization of new phases in ion-conducting nanocomposites. J. Mater. Synth. Proc. 8, 319–326.

Uvarov, N.F., Hairetdinov, E.F., Skobelev, I.V., 1996a. Composite solid electrolytes $MeNO_3$ – Al_2O_3 (Me = Li, Na, K). Solid State Ionics 86–88, 577–580.

Uvarov, N.F., Vanek, P., Yuzyuk, Y.I., Zelezny, V., Studnicka, V., Bokhonov, B.B., Dulepov, V.E., Petzelt, 1996b. Properties of rubidium nitrate in ion-conducting $RbNO_3$-Al_2O_3 nanocomposites. J. Solid State Ionics 90, 201–207.

Valenzuela, M.A., Téllez, L., Bosch, P., Balmori, H., 2001. Solvent effect on the sol–gel synthesis of lithium aluminate. Mater. Lett. 47, 252–257.

Yaroslavtsev, A.B., 2009. Composite materials with ionic conductivity: from inorganic composites to hybrid membranes. Russ. Chem. Rev. 78, 1013–1029.